

AN ANALYSIS OF OVERSHOOTING TOP LIGHTNING MAPPING ARRAY SIGNATURES IN SUPERCCELL THUNDERSTORMS

Matthew S. Elliott^{1,2,3}, Donald R. MacGorman², Terry J. Schuur^{1,2,3}, and Pam L. Heinselman²

¹Cooperative Institute for Mesoscale Meteorological Studies, University of Oklahoma
Norman, Oklahoma

²NOAA/OAR/National Severe Storms Laboratory
Norman, Oklahoma

³School of Meteorology, University of Oklahoma
Norman, Oklahoma

1. INTRODUCTION

During the afternoon of 24 May 2011, four tornadic supercells traversed central Oklahoma's (OK's) dense network of meteorological observing stations. All four of these supercells produced violent tornadoes (\geq EF-3) and hail > 6 cm in diameter during their mature stages (National Weather Service 2011, hereafter NWS11). The synoptic setup on this day was ideal for extreme weather. Just before convective initiation, surface-based convective available potential energy (SBCAPE) was $> 4500 \text{ J kg}^{-1}$ and low-level winds veered with altitude (Fig. 1). The maximum parcel level (MPL) inferred from the sounding in Fig. 1 was 18.5 km, which was a large displacement above the level of neutral buoyancy (LNB; 13.5 km; all heights given in this paper are above ground level, which was roughly 400 km above MSL). Therefore, assuming an undiluted updraft, the theoretical maximum height of the overshooting top (OT) above the LNB would be 5 km. This study utilizes data from the Oklahoma Lightning Mapping Array (OK-LMA) and local weather radars to analyze unusual VHF sources clustered in and near the OTs and their relation to the evolving kinematics and microphysics in the upper levels of supercell thunderstorms. The feasibility of OT detection using lightning mapping arrays (LMAs) for operational forecasting will also be discussed.

2. BACKGROUND

OTs are associated with convective storms having updrafts that are strong enough to penetrate the LNB. Near the LNB, OTs generally have diameters between 1 and 20 km (can be even wider in intense thunderstorms), but OT diameters decrease with height towards the MPL (Fujita 1974). Thus, the visible appearance of OTs approximates a dome-like structure. The period of an OT is wide ranging, with a lower limit of roughly 5 minutes and an upper limit of several hours. Generally, the strongest storms exhibit the largest OT diameters and the longest periods. It should be noted that long-lasting OTs are usually composed of numerous individual overshooting turrets which have much smaller diameters (< 1 km) and smaller periods (1-2 min; Fujita 1974). These overshooting turrets are a result of updraft pulses lower in the storm. If the pulses occur frequently enough, the height of the OT may appear to remain relatively stationary, giving a false illusion that the updraft pulse remains constant through time.

The presence of OTs in thunderstorms often indicates hazardous weather (e.g., large hail, tornadoes) is occurring at the surface (Fujita 1972; Reynolds 1980; Adler et al. 1985; Brunner et al. 2007). Furthermore, Darrach (1978) showed the probability of severe weather increases exponentially with increasing overshoot height. Due to the relatively strong correlation between OTs and severe weather, OT detection has become important in operational nowcasting. Current methods of OT detection involve observations from satellites, using visible and/or infrared wavelengths (Bedka et al. 2010; Bedka 2011). However, satellite observations of OTs present several complications. First and

Corresponding author address: Matthew S. Elliott
University of Oklahoma/School of Meteorology
National Weather Center
WRDD, Rm. 4340C
120 David L. Boren Blvd., Norman, OK, 73072
E-mail: Matthew.S.Elliott-1@ou.edu

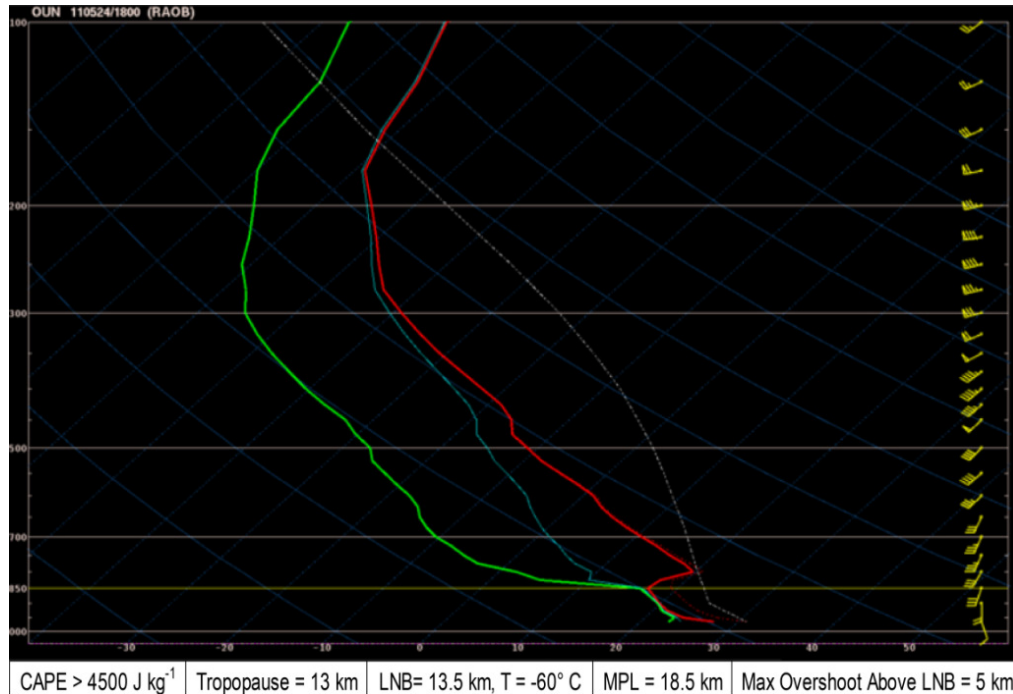


Fig. 1. The 1800 UTC, 24 May 2011 OUN modified atmospheric sounding. The environmental temperature (red line), virtual temperature (red dotted line), wet bulb temperature (blue line), and dewpoint temperature (green line) are plotted with respect to pressure. The white dotted line represents the virtual temperature of the lifted parcel according to parcel theory. The vertical wind profile is plotted using wind barbs (kt). Also included along the bottom of the image are select thermodynamic variables associated with the upper levels of thunderstorms.

foremost, in normal scanning mode, current geostationary satellites only update images every 15-30 min. Thus, the period of most OTs is less than the update time for images. Second, while visible satellite imagery has a relatively high-resolution (~ 1 km), it can be used only during the day, limiting its effectiveness. Lastly, while infrared satellite imagery can be used during both day and night, its resolution is coarse enough that many OTs with smaller radii often cannot be detected.

Soon after the installation of lightning mapping arrays (LMAs), observations of unusual emissions of very high frequency (VHF) radiation in and near OTs were reported (Krehbiel et al. 2000; MacGorman et al. 2008; Emersic et al. 2011). These electrical discharges can usually be described as continual emissions of VHF radiation, which are isolated in time and exhibit no systematic progression of development from an initiation region. Emissions typically occur at a rate on the order of a few sources per second for a period of several minutes to hours. This small VHF source rate contrasts with rates at lower altitudes, which tend to be much larger and can be as large as thousands of sources per second (cf. Figs. 2a,b). Yet clusters of VHF sources typically

form a secondary maximum of source density within or near the OT (which we will call OT LMA signatures; Fig. 2c), and individual sources appear not to be associated with flashes lower in the storm. It has been suggested that these discharges may be caused by small regions of enhanced electric field produced as upper screening-layer charge is folded by turbulent eddies closer to the internal charge lofted into the OT by intense updrafts (Emersic et al. 2011).

3. INSTRUMENTATION AND METHODOLOGY

Observations of total lightning were obtained from the OK-LMA network (MacGorman et al. 2008). On 24 May 2011, the OK-LMA network consisted of 10 ground-based measurement stations located in central OK. This array of sensors measures the electromagnetic radiation emitted by lightning. LMA sensors can detect one pulse approximately every 80 μ s and thus locate up to 12,000 s^{-1} . The time and three-dimensional location of radiation sources are determined by performing a least squares fit of measured differences in the time-of-arrival of signals received at six or more receiving stations, synchronized with Global Positioning System time (Rison et al. 1999). However, to

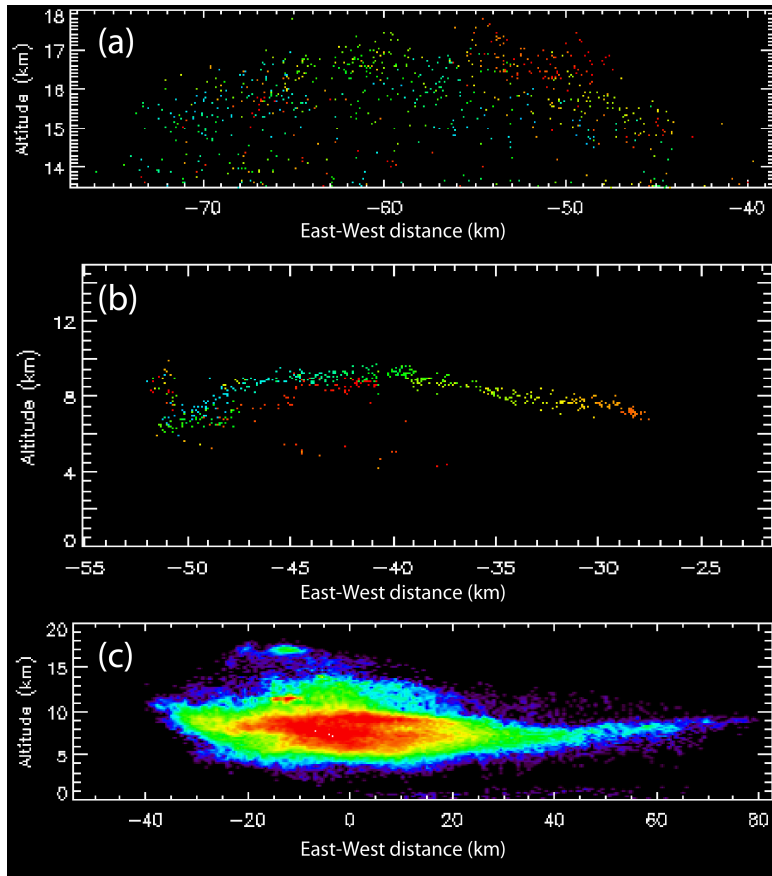


Fig. 2. (a) East-west vs altitude plot of VHF sources illustrating activity in the OT during a 10-minute period (20:10-20:20 UTC, 24 May 2011). A total of 777 sources were detected throughout this period. (b) East-west vs altitude plot of VHF sources from a typical cloud flash, lasting 470 ms (20:13:14.4-20:13:14.87 UTC, 24 May 2011). A total of 612 sources were detected for this flash. Note the difference in horizontal and vertical scales in plots (a) and (b). The color scheme in plots (a) and (b) represents the time evolution, with lighter colors (e.g., blues) occurring before darker colors (e.g., reds). (c) East-west vs altitude plot of 10-minute (21:10-21:20 UTC, 24 May 2011) VHF source densities illustrating the typical structure of an OT LMA signature, as viewed from the side. The strongest signal of the OT LMA signature is located between -10 km and -15 km in the horizontal and 17-18 km in the vertical. In this plot, lighter colors represent lowest source densities and darker colors represent highest source densities. In plots (a)-(c), east-west distance is measured from the center of the OK-LMA network. Data from Supercell A.

further increase the degrees of redundancy, VHF sources detected by fewer than eight stations or with reduced χ^2 values ≥ 2 , were not used. The location uncertainties of the mapped sources in this study are expected to be, at most, 20 m in the horizontal, 100 m in the vertical and 40 ns in time (Thomas et al. 2004).

The meteorological radars used in this study include the KOUN S-band polarimetric Weather Surveillance Radar-1988 Doppler (WSR-88D; Ryzhkov et al. 2005) and the National Weather Radar Testbed Phased-Array Radar (NWRT PAR; Zrnić et al. 2007). Both radars are located in OK. Since the KOUN radar has been upgraded to include polarimetric capabilities, in addition to measuring conventional radar

variables such as reflectivity (Z_H) and radial velocity (V_r), it also measures differential reflectivity (Z_{DR}), cross-correlation coefficient (ρ_{HV}), and differential phase (Φ_{DP}). In this study, these additional variables were used to classify hydrometeor type (Straka et al. 2000) and help infer features due to strong updrafts (e.g., Z_{DR} columns, Z_{DR} rings; Kumjian and Ryzhkov 2008). The NWRT PAR is an S-band (9.4-cm), electronically steered phased array radar system (Zrnić et al. 2007). One key advantage of the NWRT PAR is its high-temporal-resolution sampling (≤ 1 min for a 90° sector volume scan). For this case, data were collected using an adaptive scanning strategy that contained 19 elevation angles ranging from 0.5° to 52.9° and approximately one minute volumetric 90° sector scans.

To synthesize and analyze data of different formats alongside one another, the Warning Decision Support System-Integrated Information (WDSSII; Lakshmanan et al. 2006, 2007) software was used. Using WDSSII, plan-position indicator (PPI), range-height indicator (RHI), constant altitude plan-position indicator (CAPPI), and vertically integrated lightning mapping array (VILMA) plots were generated and analyzed. Thermodynamic profiles were created using the Skew-T/Hodograph Analysis Research Program (NSHARP; Hart and Korotky 1991) and modified with Oklahoma Mesonet surface data (temperature and mixing ratio). Lastly, New Mexico Tech's XLMA program was used to dissect the observed OT LMA signatures, determine the temporal evolution of the maximum height of VHF sources, and create plots of VHF radiation.

4. OBSERVATIONS

All four of the supercell storms on 24 May 2011 had extensive time periods during which OT LMA signatures were clearly discernible in OK-LMA data. Nonetheless, the cyclic supercell (we will call this Supercell A) that produced the EF-3 tornado near Lookeba (20:31–20:46 UTC; NWS11) and the violent EF-5 tornado near El Reno and Piedmont (20:50–22:35 UTC; NWS11) is the primary focus of this study, because it passed almost directly over the LMA network and was also well positioned for polarimetric and phased-array radar observations. However, a few observations from the storm (Supercell B) that produced the EF-4 tornado near Chickasha (22:06–23:01 UTC; NWS11) will also be presented.

4.1 Temporal Evolution of the OT LMA Signatures

Observations of Supercell A indicate it exhibited a quasi-steady OT LMA signature persisting with a few brief interruptions for more than two hours (19:52:35–22:10 UTC; Figs. 3a–g and 4a–g). It is likely that the OT LMA signature lasted longer, but storm mergers prevented accurate observations after 22:10 UTC. The initial penetration of VHF sources above the LNB occurred at 19:52:35 UTC and reached an altitude of 17.4 km by 19:55:50 UTC, before leveling off (Fig. 3a). Thus, the initial pulse was associated with a rise rate of approximately 20 m s⁻¹. Additionally, the initial pulse occurred 14 minutes before the first tornado warning (20:07

UTC; NWS11) and approximately 37 minutes before the first tornado was reported (20:31 UTC; NWS11). A few minutes later, at 19:57 UTC, a secondary pulse emerged from the LNB, approximately 15 km to the east of the initial pulse (Fig. 3a). This new surge reached 15.6 km before leveling off by 19:58 UTC. Accordingly, the rise rate for this surge was 35 m s⁻¹. By 20:00 UTC the second pulse had become dominant, with the first pulse no longer evident in OK-LMA data. Exploiting the high-temporal-resolution sampling of the NWRT PAR reveals the VHF pulses correlate well both spatially and temporally with upward surges in reflectivity throughout the two hour period. One particular example (not shown) evident in PAR data was an upward surge in reflectivity that was co-located with the initial VHF pulse and reached the LNB sometime between the 19:51:44 UTC scan and the 19:52:44 UTC scan. After 20:00:49 UTC, this surge in reflectivity began to dissipate rapidly, corresponding to the dissipation of the initial VHF OT LMA signature.

After a series of successively higher oscillations, the VHF sources reached a maximum height of 18.2 km (4.7 km above the LNB) at 20:53 UTC (Fig. 5). This was approximately 3 minutes after the El Reno/Piedmont tornado was first reported (NWS11). Analyses of KOUN polarimetric radar data (not shown) reveal a significant Z_{DR} column which peaked in height a few minutes (20:51:12 UTC) before the VHF height maxima. The Z_{DR} column extended to a height of 9 km, which was well above the freezing level (~4.4 km) and was located almost directly below the OT LMA signature. Z_{DR} values throughout the column were greater than 3 dB and pockets of ρ_{hv} values near the top of the column were as low as 0.8. The column of high Z_{DR} and the local relative minimum in ρ_{hv} suggest large precipitation particles were being lofted by a deep and intense updraft.

Oscillations in maximum height continued over the next hour and twenty minutes, but during this phase, the maximum crest in height steadily decreased (Fig. 5). One particular period of interest during the declining stage of the OT LMA signature occurred from approximately 21:14:40 UTC to 21:22:10 UTC (Figs. 4b,c). During this period, the majority of VHF sources were located near the upper cloud boundary instead of being spread throughout the entire depth of the OT, as was seen during previous times. It does not appear that this cluster was associated with a rising maximum of

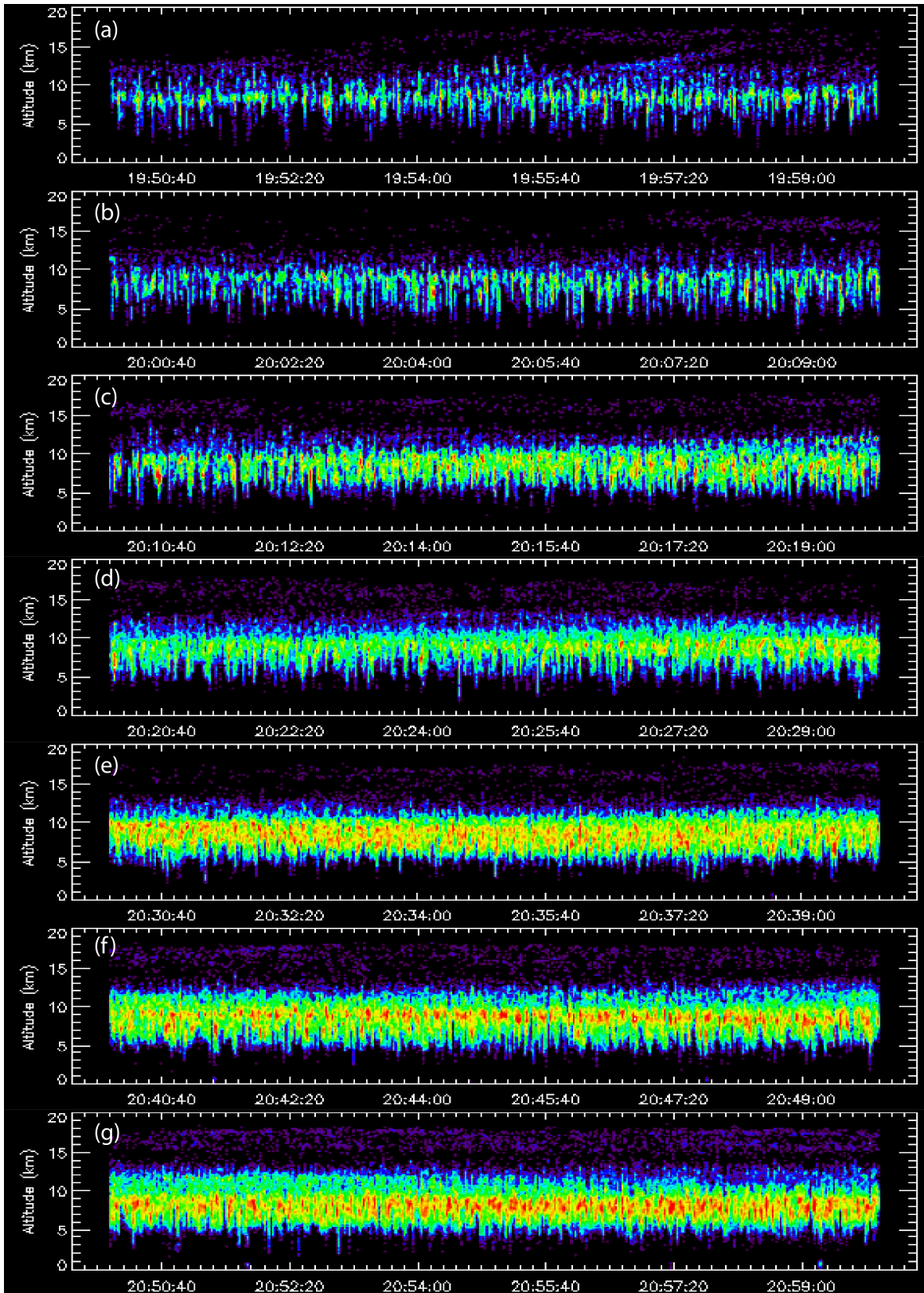


Fig. 3. (a)-(g) Time-height plots of VHF source densities for Supercell A, from 19:50-21:00 UTC, 24 May 2011. Each plot consists of a 10-minute period. Lighter colors represent lowest source densities and darker colors represent highest source densities.

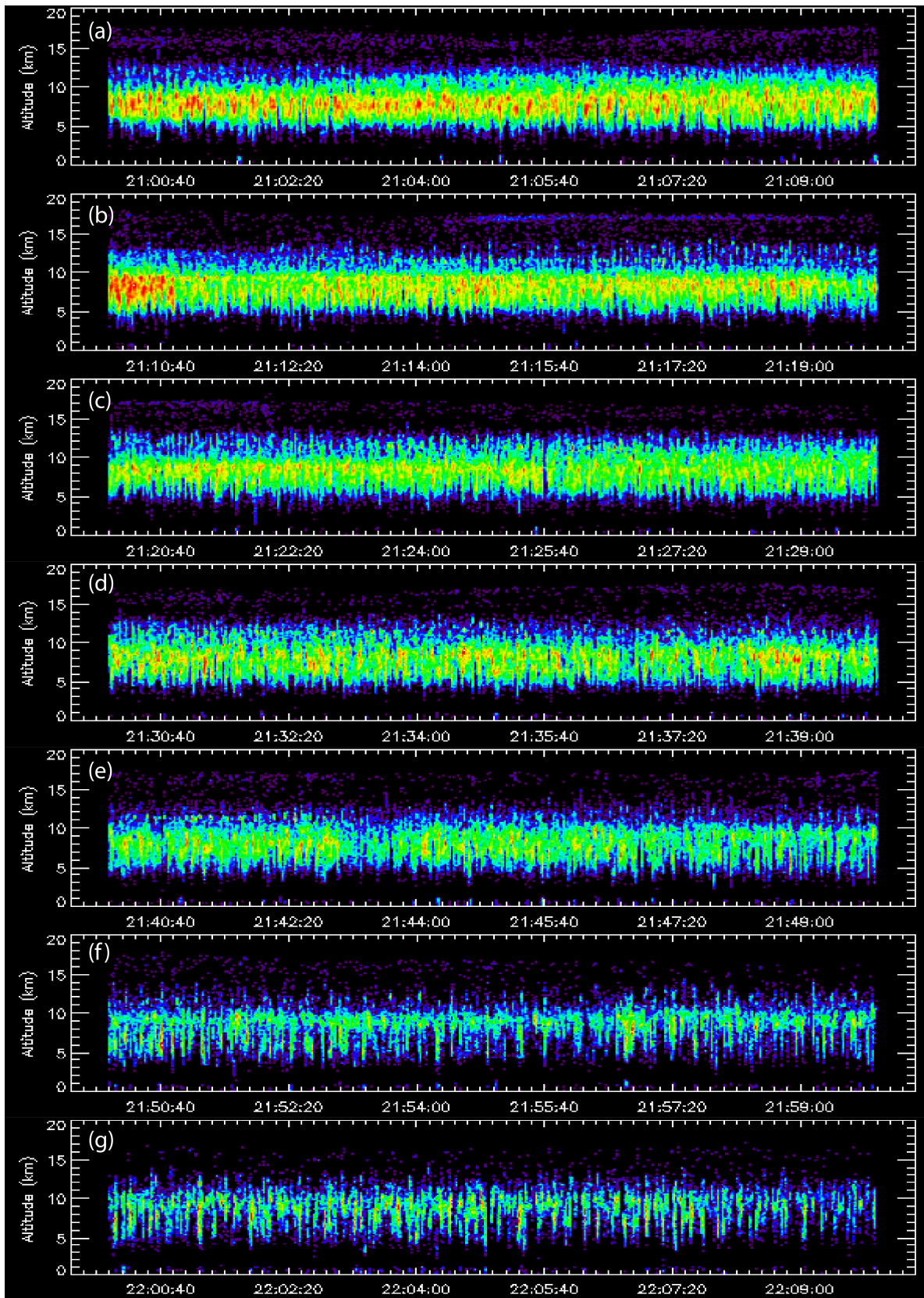


Fig. 4. (a)-(g) Same as in Fig. 3, except from 21:00-22:10 UTC, 24 May 2011.

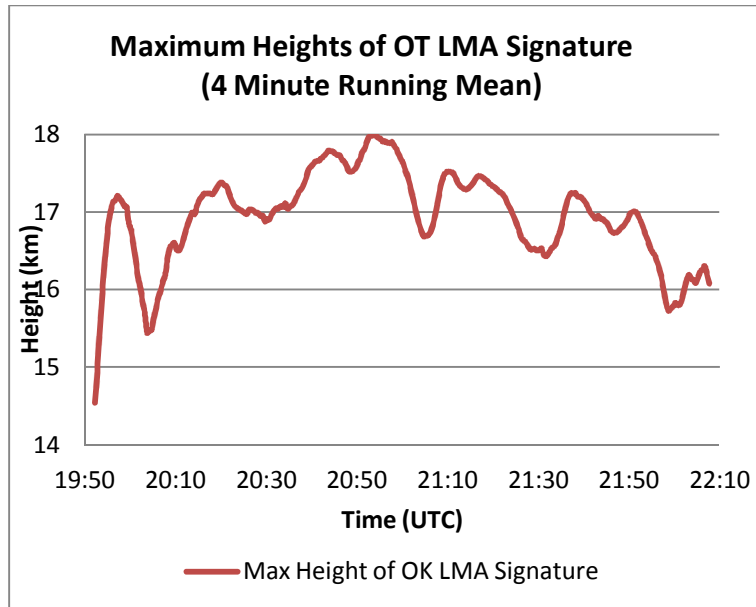


Fig. 5. Time-height plot illustrating the maximum height of VHF sources associated with the OT LMA signature in Supercell A (19:52-20:08 UTC, 24 May 2011). Values were determined by imposing a 4-minute running mean on the maximum height of VHF sources during 15 second periods.

VHF source density from lower altitudes; instead it seemed to materialize between 16.5 km and 17.5 km, with little or no oscillation during its occurrence. As demonstrated in Fig. 6, there were times when a considerable distance existed between sources clustered near the upper boundary and flashes lower in the storm. Occasionally, the vertical separation was as much as 5 km, indicating sources in the OT appear to be separate from flashes lower in the storm and not directly linked to them.

The first obvious appearance of an OT LMA signature in Supercell B occurred following a pulse that emerged from the LNB at 21:48:40 UTC and reached an altitude of 18 km by 21:52:20 UTC. Thus, the inferred rise rate was 16 m s^{-1} . The OT LMA signature was observed to occur roughly one minute before the first issued tornado warning (21:50 UTC) and 17 minutes before the first report of a tornado (22:06 UTC; NWS11). Unlike Supercell A, the OT LMA signature in Supercell B was much less pronounced, remaining at a much lower altitude ($< 16 \text{ km}$) throughout its existence. At times, the OT LMA signature even seemed to dissipate, only to return a few minutes later. Beginning at 23:00 UTC, the maximum height of VHF sources descended from 15.7 km to 13 km, as the supercell was engulfed by the trailing cold front. The tornado lifted during this period at 23:01 UTC (NWS11).

4.2 High Altitude Flashes

Occasionally, small nearly vertical flashes were observed to initiate above the LNB. These small flashes usually consisted of fewer than 100 VHF sources and typically had spatial and temporal dimensions less than $1 \text{ km} \times 1 \text{ km} \times 1 \text{ km}$ and 250 ms, respectively. This compact burst of VHF sources in the OT is in stark contrast to the sparse, but continual, VHF sources typically detected within the OT. The majority of these small flashes were observed to propagate downward, often terminating at or slightly below the LNB. Fig. 7 illustrates one of the high altitude flashes which occurred on 24 May 2011. While in a sense this flash represents an extreme example, due to the very high altitude of its initiation and termination (14.85 km and 14.15 km, respectively), in many respects its characteristics are typical of high altitude flashes. For example, only 44 sources were detected from this flash, which lasted 150 ms, and its spatial dimensions were approximately $100 \text{ m} \times 500 \text{ m} \times 700 \text{ m}$. Throughout the lifetimes of Supercells A and B, only a handful of flashes were observed to be initiated above the LNB. On the other hand, immediately below the LNB, brief compact flashes were more common. This implies that the conditions needed to produce for compact flashes at high altitudes are rarely observed to occur within the OT.

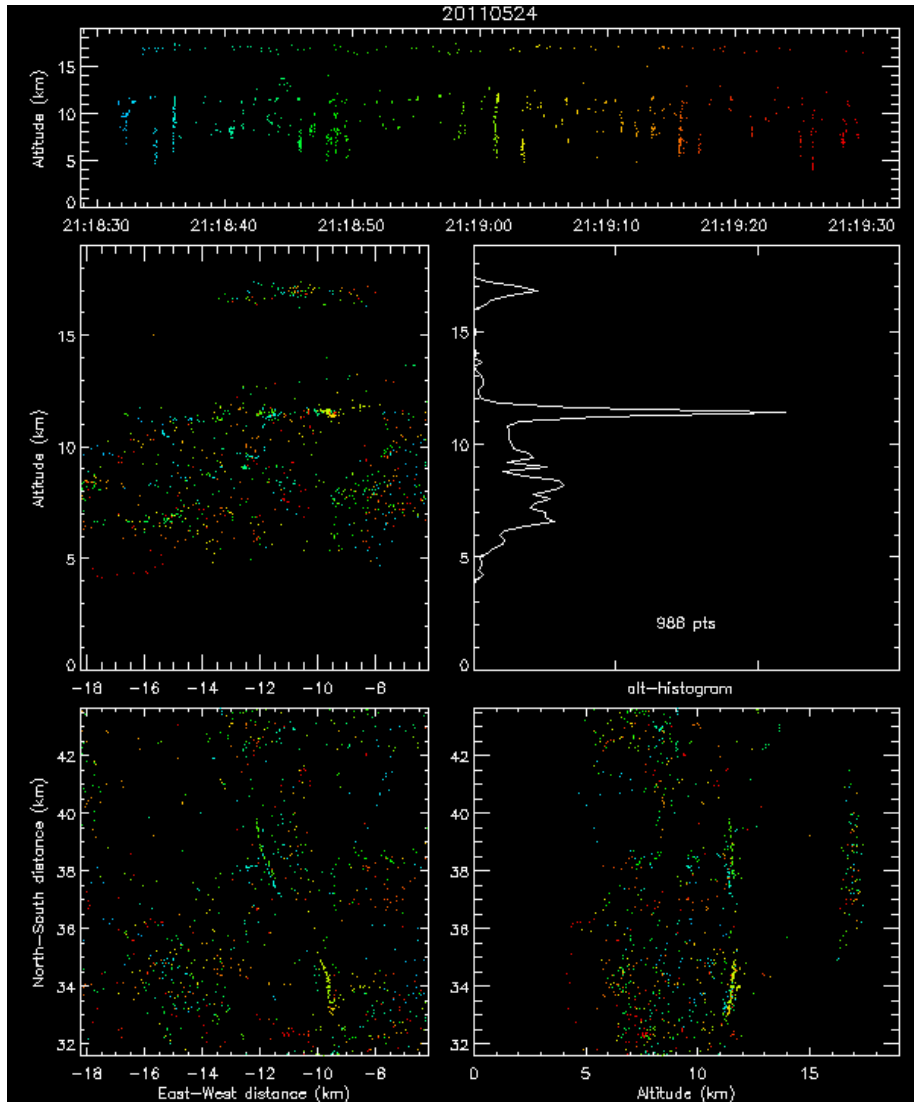


Fig. 6. 1-minute (21:18:30-21:19:30 UTC, 24 May 2011) time-height (upper), east-west vs altitude (middle-left), plan view (lower-left), and north-south vs altitude (lower-right) plots from Supercell A illustrating the discontinuity between sources in the OT (located above 15 km) and flashes lower in the storm (below 13.5 km). The color scheme represents the time evolution, with lighter colors (e.g., blues) occurring before darker colors (e.g., reds). Distances are measured from the center of the OK-LMA network.

4.3 The Use of LMA Array Signatures for OT Detection

As mentioned previously, satellite imagery is the main tool used by operational forecasters for OT detection. However, the infrequency of its updates and its coarse resolution imply a need for alternate OT detection methods. While it remains unclear if all storms with OTs exhibit OT LMA signatures, we are fairly certain that OT LMA signatures only occur in the presence of OTs. Therefore, it seems reasonable to conclude LMA networks could be used for OT detection. Particular advantages of LMA

networks include ultra-fine resolution to determine the spatial extent of the overshoot and the ability to detect changes in storm top heights as they transpire. For comparison of OT detection using satellites and LMAs, the authors created a specialized product in WDSSII. This product modified the 1-minute VILMA feature to vertically integrate the number of sources between 15 km and 18 km, and it enabled the OT LMA signatures to be easily located. As shown in Figs. 8 and 9, the OT LMA signature corresponds well with the OT detected in satellite imagery (the OT in satellite imagery is slightly shifted to the west, because of the parallax effect).

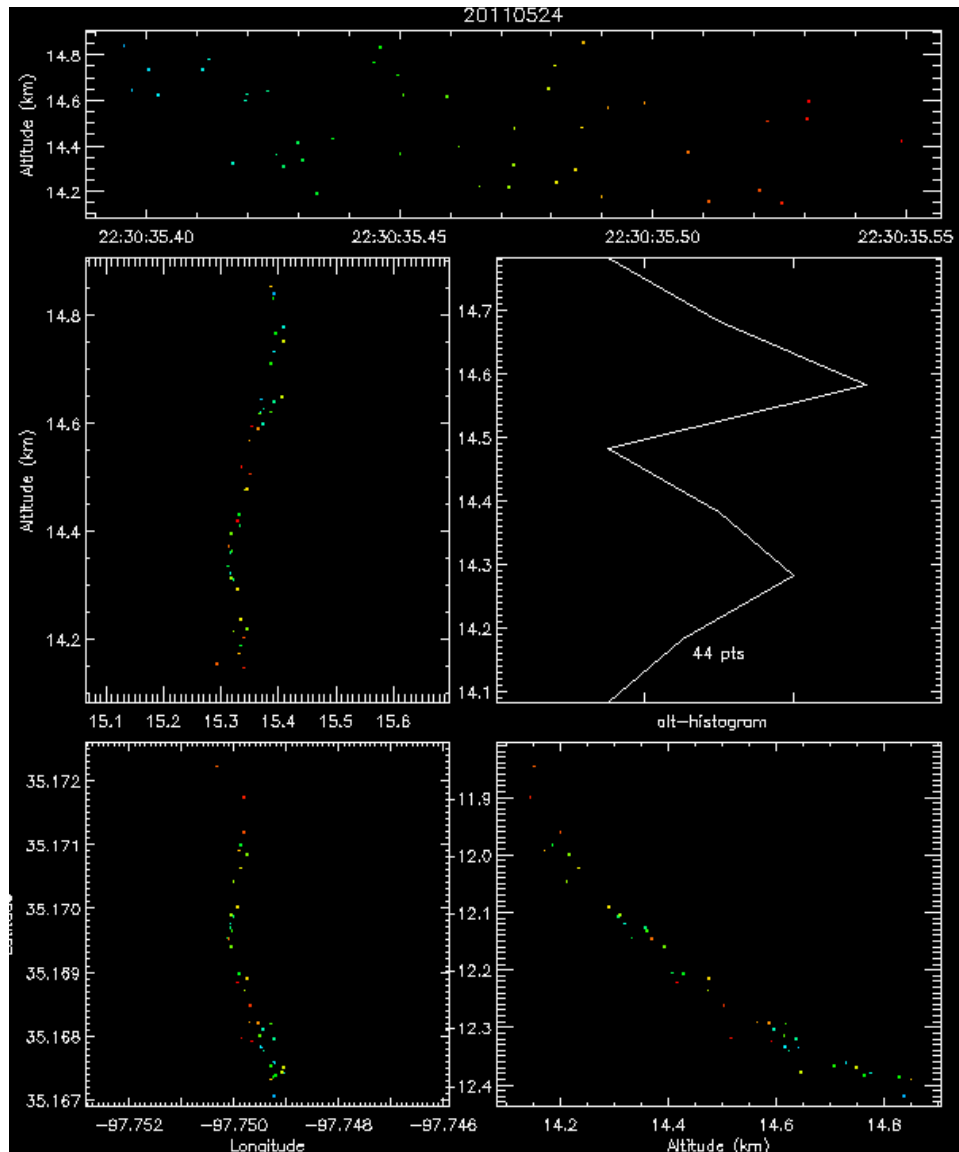


Fig. 7. A 151 ms (22:30:35.39-22:30:35.55 UTC, 24 May 2011) plot from Supercell B, illustrating an example of a high altitude flash. Panel representations and color schemes are the same as in Fig. 6, except plan view plot has longitude on the abscissa and latitude on the ordinate.

5. SUMMARY AND CONCLUSIONS

The afternoon of 24 May 2011 was no ordinary day across central OK, with four supercell thunderstorms producing several violent tornadoes. This study examined two of these supercells in an effort to provide observations of OT LMA signatures, as well as to assess the relationship between OT LMA signatures and evolving kinematics and microphysics in supercell thunderstorms. It was shown that the supercell storm which produced the EF-5 tornado near El Reno and Piedmont exhibited a quasi-steady OT LMA signature that

persisted for more than two hours. During this time, several oscillations were observed in the maximum height of VHF sources. High-temporal-resolution NWRT PAR data indicated that the oscillations in maximum VHF source height corresponded well with surges in reflectivity height. Furthermore, polarimetric radar data from KOUN indicate pockets of relatively low ρ_{hv} values atop deep Z_{DR} columns, which were located almost directly below the OT LMA signature. During the most extreme cases, the Z_{DR} columns reached heights up to 9 km, indicating deep updrafts and thus the likelihood for significant OTs.

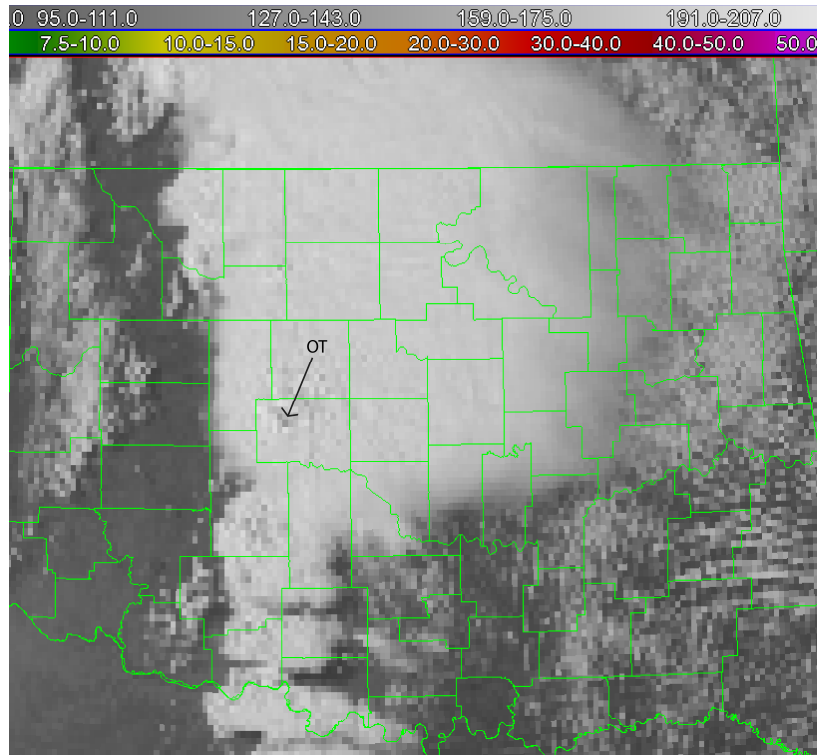


Fig. 8. Visible satellite imagery from 21:15 UTC, 24 May 2011 with an arrow indicating the location of the OT in Supercell A.

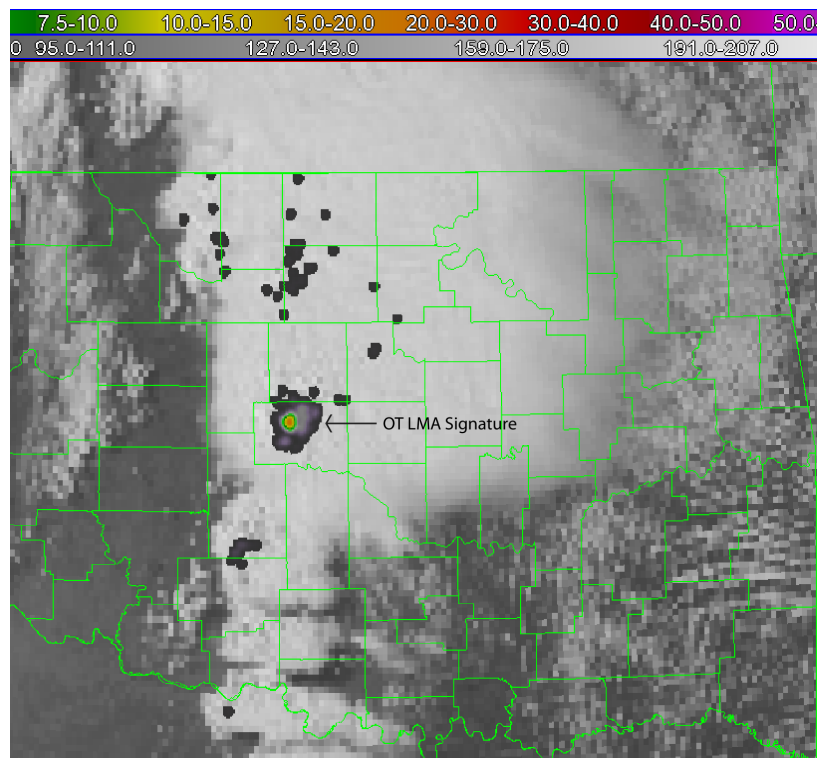


Fig. 9. Modified 1-minute VILMA (between 15 km and 18 km) from 21:15 UTC, May 24 2011 overlaid on visible satellite imagery (same as in Fig. 8) with an arrow indicating the location of the OT LMA signature in Supercell A (cf. Fig. 8). Highest values near the center of the OT LMA signature are approximately 20 sources per min per km².

In future investigations, the authors will build upon this study to further evaluate the relationship between OT LMA signatures and their parent thunderstorm's characteristics. Research goals include analyzing different storm types (e.g., supercells, MCSs, pulse-type) during different seasons to assess if preferred patterns to OT LMA signatures exist. Additionally, we plan to investigate in greater detail the high altitude flashes occurring above the LNB to determine if they are simply manifestations of flashes lower in the storm or a different phenomenon altogether. Lastly, we will continue to evaluate the feasibility of using emissions of VHF radiation to improve detection of OTs.

6. ACKNOWLEDGEMENTS

The authors would like to acknowledge support for this work from the National Science Foundation Grant ATM-0924621. We would also like to thank Kevin Manross and Kristin Kuhlman for helping set up WDSSII and Erica Griffin for reviews of the manuscript.

7. REFERENCES

- Alder, R. F., M.J. Markus, and D. D. Fenn, 1985: Detection of severe Midwest thunderstorms using geosynchronous satellite data. *Mon. Wea. Rev.*, **113**, 769-781.
- Bedka, K. M., J. Brunner, R. Dworak, W. Feltz, J. Otkin, and T. Greenwald, 2010: Objective satellite-based detection of overshooting tops using infrared window channel brightness temperature gradients. *J. Appl. Meteor. Climatol.*, **49**, 181-202.
- , 2011: Overshooting cloud top detections using MSG SEVIRI infrared brightness temperatures and their relationship to severe weather over Europe. *Atm. Res.*, **99**, 175-189.
- Brunner, J. C., S. A. Ackerman, A. S. Bachmeier, and R. M. Rabin, 2007: A quantitative analysis of the enhanced-V feature in relation to severe weather. *Wea. Forecasting*, **22**, 853-872.
- Darrah, R. P., 1978: On the relationship of severe weather to radar tops. *Mon. Wea. Rev.*, **106**, 1332-1339.
- Emersic, C., P.L. Heinselman, D.R. MacGorman, E. C. Bruning, 2011: Lightning activity in a hail-producing storm observed with phased-array radar. *Mon. Wea. Rev.*, **139**, 1809-1825.
- Fujita, T. T., 1972: Tornado Occurrences related to overshooting cloud-top heights as determined from ATS pictures. *SMRP Res.*, Paper 97, 32 pp.
- , 1974: Overshooting thunderheads observed from ATS and Learjet. *SMRP Res.*, Paper 117, 29 pp.
- Hart, J.A., and W. Korotky, 1991: The SHARP workstation vl.50 users guide. NOAA/National Weather Service. 30 pp. [Available from NWS Eastern Region Headquarters, 630 Johnson Ave., Bohemia, NY 11716.
- Krehbiel, P.R., R.J. Thomas, W. Rison, T. Hamlin, J. Harlin, and M. Davis, 2000: GPS-based mapping system reveals lightning inside storms. *Eos, Trans. Amer. Geophys. Union*, **81**, 21-25.
- Kumjian, M. R., and A. V. Ryzhkov, 2008: Polarimetric signatures in supercell thunderstorms. *J. Appl. Meteor. Climatol.*, **48**, 1940–1961.
- Lakshmanan, V., T. Smith, K. Hondl, G.J. Stumpf, and A. Witt, 2006: A real-time, three-dimensional, rapidly updating, heterogeneous radar merger technique for reflectivity, velocity, and derived products. *Wea. Forecasting*, **21**, 802-823.
- , —, G. J. Stumpf, and K. Hondl, 2007: The Warning Decision Support System-Integrated Information. *Wea. Forecasting*, **22**, 596-612.
- MacGorman, D. R., W. D. Rust, T. J. Schuur, M. I. Biggerstaff, J. M. Straka, C. L. Ziegler, E. R. Mansell, E. C. Bruning, K. M. Kuhlman, N. R. Lund, N. S. Biermann, C. Payne, L. D. Carey, P. R. Krehbiel, W. Rison, K. B. Eack, and W. H. Beasley, 2008: TELEX: The Thunderstorm Electrification and Lightning Experiment. *Bull. Amer. Meteor. Soc.*, **89**, 997-1013.
- National Weather Service, 2011: Information for the tornado outbreak of May 24, 2011. [Available online at <http://www.srh.noaa.gov/oun/?n=events-20110524>]
- Reynolds, D. W., 1980: Observations of damaging hailstorms from geosynchronous satellite digital data. *Mon. Wea. Rev.*, **108**, 337-348.
- Rison, W., R. J. Thomas, P.R. Krehbiel, T. Hamlin, and J. Harlin, 1999: A GPS-based three-dimensional lightning mapping system: Initial observations in central New Mexico. *Geophys. Res. Lett.*, **26**, 3573-3576.
- Ryzhkov, A. V., S. E. Giangrande, and T. J. Schuur, 2005: Rainfall estimation with a

- polarimetric prototype of WSR-88D. *J. Appl. Meteor.*, **44**, 502-515.
- Straka, J. M., D. S. Zrnić, and A. V. Ryzhkov, 2000: Bulk hydrometeor classification and quantification using polarimetric radar data: Synthesis of relations. *J. Appl. Meteor.*, **39**, 1341-1372.
- Thomas, R., P. Krehbiel, W. Rison, S. Hunyady, W. Winn, T. Hamlin, and J. Harlin, 2004: Accuracy of the lightning mapping array. *J. Geophys. Res.*, **109**, D14207, doi:10.1029/2004JD004549.
- Zrnić, D. S. J. F. Kimpel, D. E. Forsyth, A. Shapiro, G. Crain, R. Ferek, J. Heimmer, W. Benner, T. J. McNellis, R. J. Vogt, 2007: Agile-beam phased array radar for weather observations. *Bull. Amer. Meteor. Soc.*, **88**, 1753-1766.